

PACS numbers: 81.15.Cd, 73.61.Le, 61.05.Cp, 78.20.Ci, 68.37.Ps

## MAGNETRON SPUTTERED Al-ZnO THIN FILMS FOR PHOTOVOLTAIC APPLICATIONS

**J.R. Ray<sup>1</sup>, M.S. Desai<sup>1</sup>, C.J. Panchal<sup>1</sup>, P.B. Patel<sup>2</sup>**

<sup>1</sup> Applied Physics Department, M.S. University of Baroda,  
390001, Vadodara, India  
E-mail: [cjpanchal\\_msu@yahoo.com](mailto:cjpanchal_msu@yahoo.com)

<sup>2</sup> Department of electronics, Sardar Patel University,  
388120, Vallabh Vidyanagar, India

*The optimization process of the RF magnetron sputtered Al – doped ZnO (AZO) thin films was carried out by studying its structural, optical, electrical, and morphological properties at different RF power and different working pressures for its use as a front-contact for the copper indium diselenide (CIS) based thin film solar cell. The structural study suggests that the preferred orientation of grains along the (002) plane having a hexagonal structure of the grains. The optical and electrical properties suggest that the films show an average transmission of 85 % and a resistivity of the order of  $10^{-4}$   $\Omega$ cm. The morphology analysis suggests the formation of packed grains having a homogeneous surface.*

**Keywords:** RF MAGNETRON SPUTTERING, Al-ZnO THIN FILM, STRUCTURAL, OPTICAL, ELECTRICAL, MORPHOLOGICAL CHARACTERIZATION.

*(Received 04 February 2011, in final form 14 October 2011)*

### 1. INTRODUCTION

Thin films, which can be used as window layers in many optoelectronic devices, need to be transparent to the visible range of the light spectrum and be conductive enough. To date, the industry standard for transparent conducting oxide (TCO) is tin-doped indium-oxide (ITO). This material has a low resistivity of  $\sim 10^{-4}$   $\Omega$ cm and a transmission greater than 80 %. However, in the field of solar cells, Al-doped ZnO (AZO) thin films have caught the attention for its use as a window layer because of its low cost and wide availability of its constituent raw materials compared to ITO. In the AZO thin films, the textured surface structure formation is easy compared to that in ITO [1], which increases the light trapping capability of the front surface of the solar cell and hence reduces the reflection losses. For the deposition of the AZO, the most commonly used technique is by radio frequency (RF) magnetron sputtering due to its high reproducibility [2, 3]. Besides, it permits the deposition be carried out at low substrate temperatures, leading to smooth films with a good surface uniformity. Nowadays, there is an increasing interest in reducing the substrate temperature for many applications in order to minimize the inter-diffusion processes on prior deposited materials. Additionally, the use of flexible substrates such as plastic polymers replacing the conventional glass substrates becomes of great interest in the photovoltaic field as they contribute to cost reduction in the production processes [4].

In this study, we present the results regarding the optimization of AZO thin films deposited on soda lime glass substrate. The optimization process was performed by varying the RF power and the working pressure and studying their influence on the structural, optical, morphological, and electrical properties, in order to achieve the highest transparency and lowest resistivity films. The outcome suggested its use as a window layer in the solar cell structure.

## 2. EXPERIMENTAL

AZO thin films were optimized for the application of the Copper Indium Gallium diselenide (CIGS) thin film solar cells for the front-contact using radio frequency (RF) magnetron sputtering system (HUTTINGER Elektronik, 600 W, Germany). We have used a 50 mm diameter ceramic target of ZnO : Al<sub>2</sub>O<sub>3</sub> (98 % : 2 % wt). For the deposition of AZO thin films the vacuum chamber was first evacuated with a base pressure of  $1 \times 10^{-5}$  Torr using a vacuum coating unit (HINDHIHVAC, model – 15F6, Bangalore). By using the Ar gas flow, the pressure was controlled roughly and then by throttling the baffle valve a fine control on the chamber pressure was achieved. AZO thin films were grown on soda lime glass substrates. The glass substrates with a dimension of  $50 \times 50 \text{ mm}^2$  were cleaned ultrasonically in a vapour of acetone, ethanol, and deionized (DI) water, followed by drying in blowing nitrogen. At the time of the deposition, we rotate the substrate at a speed of 40 rpm for the uniform coating of AZO thin film. Before the deposition, pre-sputtering was applied for 5 minutes at 5 mTorr pressure to remove the surface contamination of the AZO target. The source to substrate distance was kept 70 mm for all AZO deposition. The thickness of all AZO films was kept constant viz. 300 nm, which was measured in-situ by using the quartz crystal thickness monitor. No any external heat treatment applies during the time of the deposition.

Structural, optical, and electrical properties of RF magnetron sputtered AZO thin films were analyzed using an X-ray diffraction (XRD) (D8 ADVANCE, Bruker AXS, USA), a UV-VIS spectrophotometer (Thermo Fisher Scientific, USA), and a four-point probe method using Keithley 2420C source meter, respectively. The films were polycrystalline in nature showing a strong preferred c-axis orientation of the (002) plane. The optimum transmittance and resistivity were achieved at 10 mTorr working pressure viz. ~ 80 % transmittance in the visible wavelength range and resistivity near to  $10^{-4} \Omega\text{cm}$ . Furthermore, the surface morphology was examined using atomic force microscopy (AFM), which showed packed grain geometry for the AZO thin films.

## 3. RESULTS

### 3.1 Effect of RF power

The XRD spectrum of the AZO target is shown in Fig. 1. Through identifications of XRD, we found that all peaks presented in the spectra are from the ZnO crystal structure [5]. The XRD spectra of AZO thin films deposited at different RF power (80 W to 150 W) using AZO target is shown in Fig. 2. We have kept the working pressure constant at 10 mTorr.

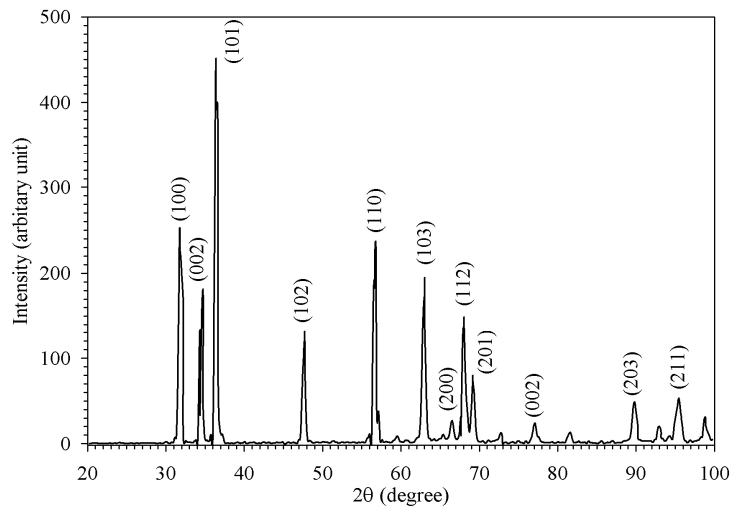


**Fig. 1** – The XRD spectra of the AZO target

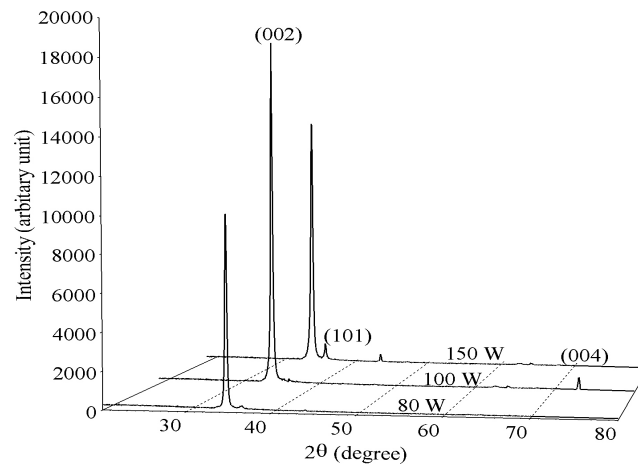


**Fig. 2** – The XRD spectra of the AZO thin films deposited at different RF power shows a preferred orientation along the (002) plane

The XRD spectra revealed a strong preferred orientation of the (002) peak indicating that the films were orientated with their axes perpendicular to the substrate plane and having a hexagonal structure [5]. Small diffraction intensity from (101) and (004) planes are also present in the XRD spectra. As the RF power vary the deposition rate also varies with it. It was increase from 1.6 Å/s to 2.8 Å/s by varying the RF power from 80 W to 150 W. From the XRD data, the average crystallite size ( $D$ ) can be evaluated by the Scherrer formula as follows [6],

$$D = \frac{0.9 \lambda}{\beta \cos \theta} \quad (1)$$

where,  $D$  is the crystalline size,  $\lambda$  is the X-ray wavelength (0.154 nm),  $\theta$  is the Bragg angle, and  $\beta$  is the full-width at half-maximum (FWHM) of the AZO (002) diffraction peak. The crystallite size increases with increasing RF power. At 150 RF power, highest crystallite size of 10.18 nm was observed.

**Table 1** – The d-spacing, FWHM, and crystallite size of AZO thin films grown at different power keeping working pressure constant at 10 mTorr

RF power (watt)	d-spacing (Å)	FWHM (degree)	Crystallite size (nm)
80	2.56	0.95	8.50
100	2.55	0.85	9.66
150	2.56	0.79	10.18

The influence of the RF power on the optical properties viz. transmission, energy band gap,  $E_g$ , and optical absorption,  $\alpha$ , of the AZO films was analyzed. Fig. 3 shows the transmission spectra of the AZO thin films deposited at different RF power i.e., from 80 W to 150 W. The average transmittance is ~ 80 % observed between 450 and 800 nm range (visible range).

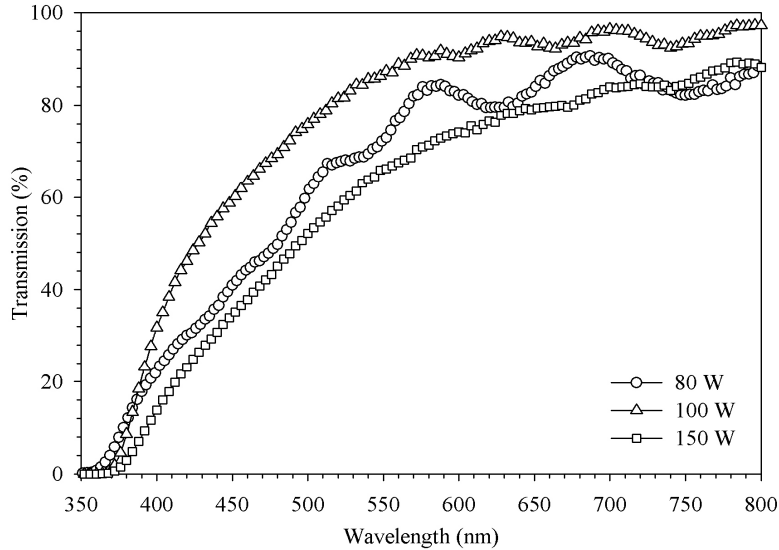


**Fig. 3** – The transmission spectra of the AZO thin films deposited at different RF power

From the optical transmission data, the value of  $\alpha$ , which provides the information of the band structure, is given by [7],

$$I = I_0 \exp(-\alpha d) \tag{2}$$

where,  $I_0$  and  $I$  denote the intensities of the incident light and the transmitted light, respectively, and  $d$  is the film's thickness in nm. By using the values of  $\alpha$ , the  $E_g$  of AZO thin films were calculated using the formula [7],

$$\alpha h\nu = (h\nu - E_g)^{\frac{1}{2}} \quad (3)$$

where,  $h\nu$  is the photon energy. The plot of  $(\alpha h\nu)^2$  versus  $h\nu$  is shown in Fig. 4 (a). The  $E_g$  can be obtained by extrapolating the straight-line portion of plots to the photon energy axis. The value of  $E_g$  for as deposited AZO films was in the range of 3.31 eV to 3.38 eV (Table 2). Fig. 4 (b) shows the variation in  $\alpha$  as a function of wavelength.

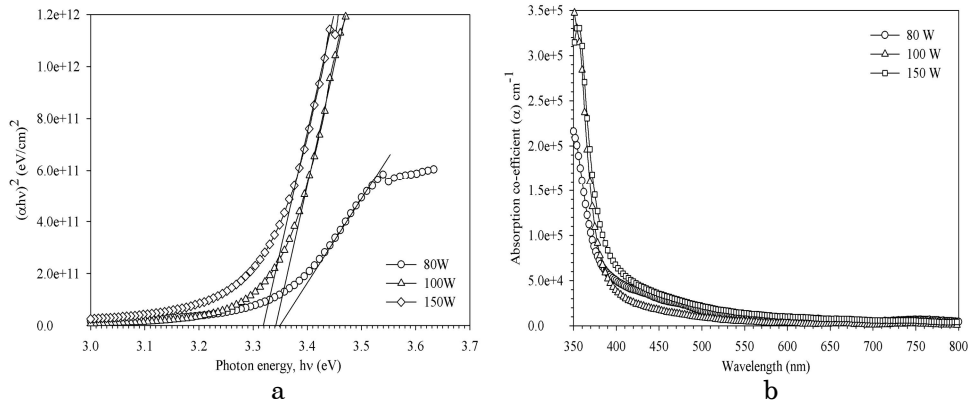


**Fig. 4** – (a) Plot of  $(\alpha h\nu)^2$  versus  $h\nu$  for AZO thin films deposited at different RF power (b) – Variation in the absorption coefficient ( $\alpha$ ) of AZO thin films deposited at different RF power

The surface morphology of the AZO thin film was observed using AFM. The morphology of the as deposited films indicates the packed AZO grains, which is shown in Fig. 5. The surface roughness (from Table 2) was 19.21 nm for 80 W and it increases to 36.77 nm when the RF power reached to 150 W.

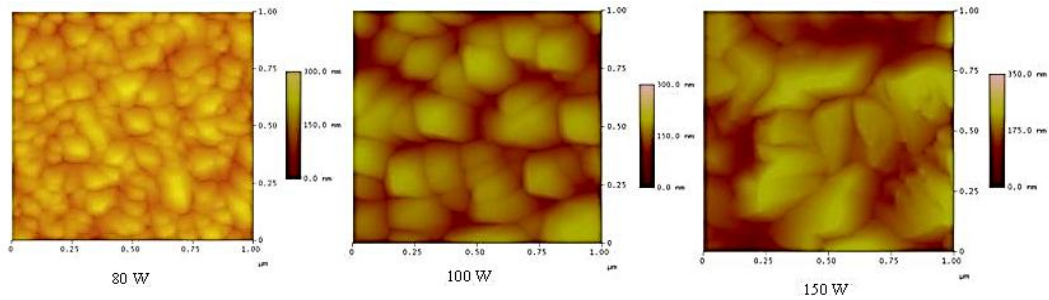


**Fig. 5** – The AFM images of the AZO thin films deposited at different RF power

For the use of AZO thin films as a window layer in the CIS thin film solar cell, it has to behave as a metallic conductor. The sheet resistance ( $R_{sh}$ ) and resistivity ( $\rho$ ) of AZO thin films grown at different RF power were measured using the four-point probe method at RT. In addition, using the hot-probe method, we observed that all the AZO thin films showed n-type

behavior. By increasing the RF power from 80 W to 150 W the  $R_{sh}$  decreases from 50 to 16  $\Omega/\square$  and the lower resistivity ( $4.8 \times 10^{-4} \Omega\text{cm}$ ) is measured at 150 W which is shown in Table 2.

**Table 2** – The variation in the values of energy band gap, sheet resistance resistivity and the surface roughness of AZO thin films, grown at 10 mTorr working pressure, as a function of RF power

RF Power (watt)	Energy band gap, $E_g$ , (eV)	Sheet resistance, $R_{sh}$ , ( $\Omega/\square$ )	Resistivity, $\rho$ , ( $\Omega\text{cm}$ )	Surface roughness (nm)
80	3.35	50	$1.5 \times 10^{-3}$	17.73
100	3.34	23	$6.9 \times 10^{-4}$	26.14
150	3.32	16	$4.8 \times 10^{-4}$	36.77

### 3.2 Effect of working pressure

To study the effect of the working pressure, on the different properties of the AZO thin films, we have deposited the AZO thin film in the working pressure range of 2 to 20 mTorr at 100 W.

By varying the working pressure, the deposition rate varies significantly. This is the key factor, which affect the properties of the thin films. In our case the deposition rate is higher (3.2  $\text{\AA}/\text{s}$ ) for lower (2 mTorr) pressure and lower (1.5  $\text{\AA}/\text{s}$ ) for higher pressure (20 mTorr). The XRD spectra of AZO thin film deposited at different working pressure (2 to 20 mTorr) at 100 W RF power is shown in Fig. 6.

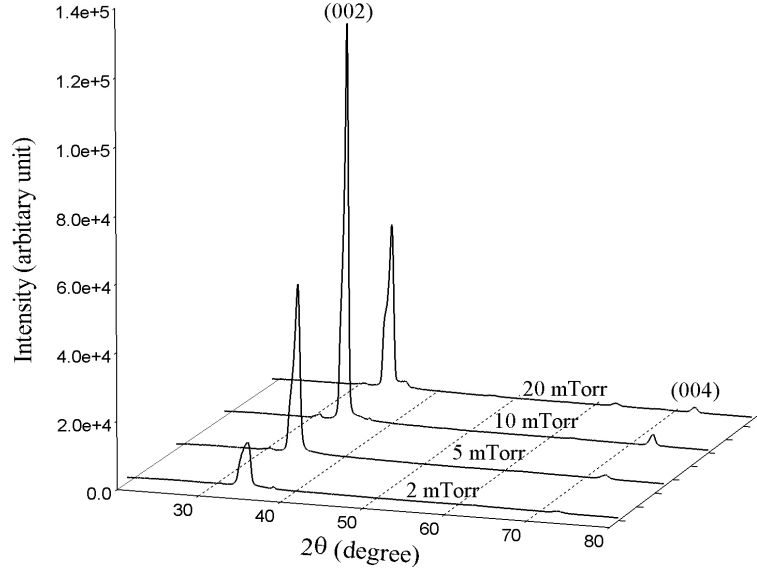


**Fig. 6** – The XRD spectra of the AZO thin films deposited at different working pressures

All AZO thin films show a preferred orientation along (002) direction. The intensity of (002) peak is observed highest at 10 mTorr working pressure and the highest crystallite size viz. 9.66 nm are tabulated in Table 3.

**Table 3** – The *d*-spacing, FWHM, and the crystallite size of the AZO thin films grown at different working pressure by keeping RF power constant at 100 W

Working pressure (mTorr)	<i>d</i> -spacing (Å)	FWHM (degree)	Crystallite size (nm)
2	2.56	0.99	8.16
5	2.55	0.96	8.47
10	2.55	0.85	9.66
20	2.557	1.000	8.14

The optical transmission spectrum of AZO thin films grown at different working pressures is shown in Fig. 7. Using the transmission data, a plot of  $(\alpha h\nu)^2$  versus  $h\nu$  and the variation in  $\alpha$  as a function of wavelength are shown in Fig. 8 (a) and (b) respectively.

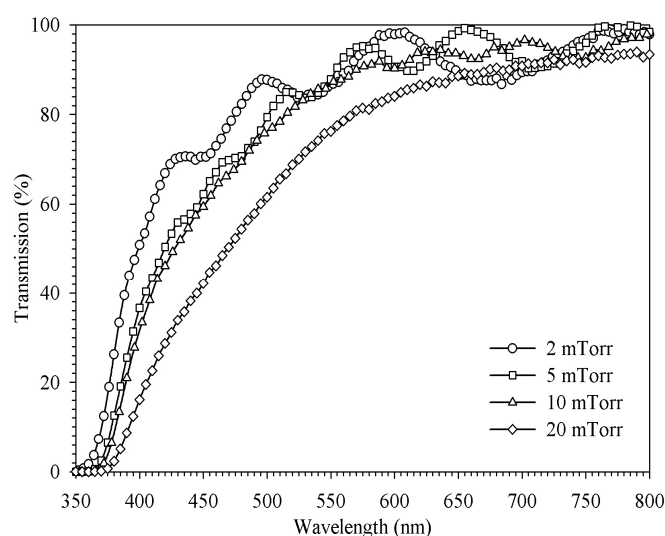


**Fig. 7** – The transmission spectra of the AZO thin films deposited at different working pressures

The influence of the working pressure is clearly seen in the transmission spectrum of AZO thin films. The transmission is ~85 % transmission and the variation in the  $E_g$  is from 3.31 eV to 3.38 eV is observed. The variation in the  $E_g$  as a function of working pressure is shown in Table 4.

Fig. 9 shows the AFM image of the AZO thin films grown at different working pressures at 100 W RF power. As we move from 2 mTorr to 10 mTorr, the surface roughness increases from 19.21 nm to 26.14 nm, respectively. On increasing the pressure further, at 20 mTorr, the roughness was 22.70 nm.

**Table 4** – The variation in the values of energy band gap, sheet resistance resistivity and the surface roughness of AZO thin films, grown at 100 W RF power, as a function of working pressure

Working pressure (mTorr)	Energy band gap, $E_g$ , (eV)	Sheet resistance, $R_{sh}$ , ( $\Omega/\square$ )	Resistivity, $\rho$ , ( $\Omega\text{cm}$ )	Surface roughness (nm)
2	3.38	50	$1.5 \times 10^{-3}$	19.21
5	3.36	37	$1.1 \times 10^{-3}$	23.29
10	3.34	23	$6.9 \times 10^{-4}$	26.14
20	3.31	29	$8.7 \times 10^{-3}$	22.70

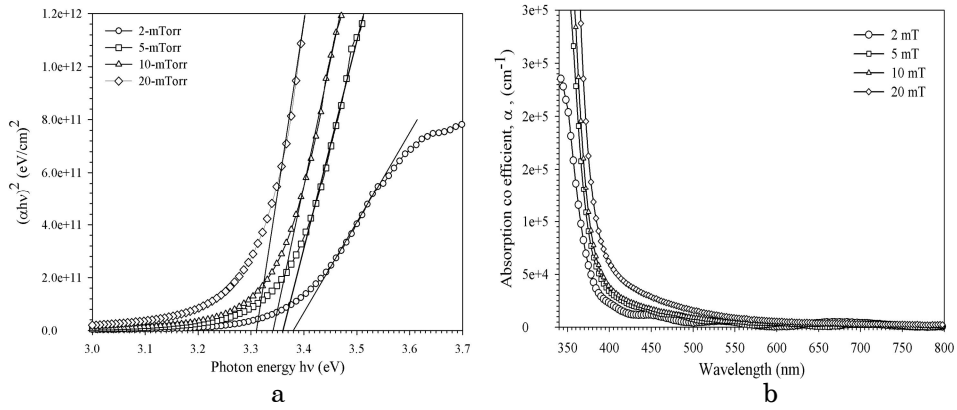


**Fig. 8** – Plot of  $(ahv)^2$  versus  $h\nu$  for AZO thin films deposited at different working pressures (a); variation in the absorption coefficient ( $\alpha$ ) of AZO thin films deposited at different working pressures (b)

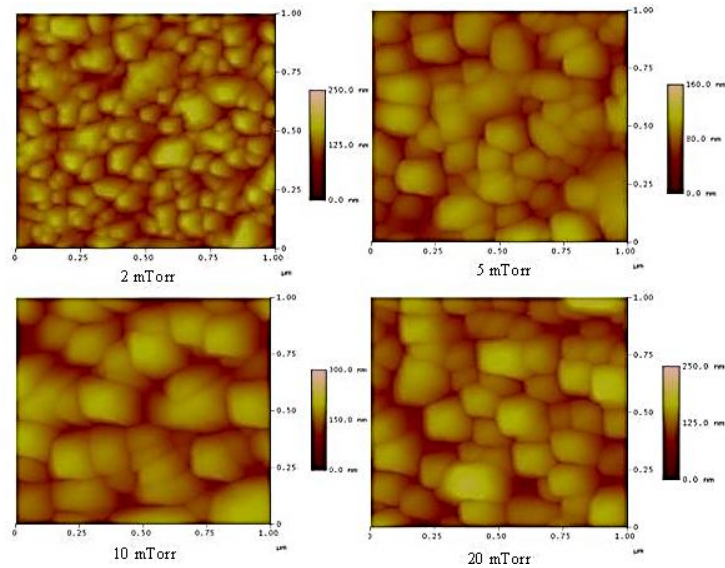


**Fig. 9** – The AFM images of the AZO thin films deposited at different working pressures

The sheet resistance and resistivity of AZO thin films grown at different pressures and measured using the four-point probe method at RT is in the range of  $10^{-3}$  to  $10^{-4}$   $\Omega\text{cm}$  and the hot-probe method suggest the *n*-type conductivity. At 10 mTorr working pressure, we observed (Table 4) lowest resistivity  $6.9 \times 10^{-4}$   $\Omega\text{cm}$ .

## 4. DISCUSSIONS OF RESULTS

### 4.1 Discussion of RF power

In RF magnetron sputtering as the RF power increases the deposition rate increases because of the highly energetic ionized argon atoms bombard on the target, which leads to increase in the ejection rate of the sputtered atoms. The XRD spectra of AZO thin films deposited at different RF power shows strong (002) diffraction peaks. Other peaks (004) with much less intensity were observed, indicating that the films are oriented with their *c* axis perpendicular to the substrate plane. The highest (002) peak value of AZO thin films was obtained at RF power of 100 W. The crystallite size of the AZO thin films was evaluated according to Scherrer relation was found to be in range of 8.50 – 10.18 nm with the varying the sputtering power from 80 W to 150 W, and a highest value, 10.18 nm, obtained at the power of 100 W. Any  $\text{Al}_2\text{O}_3$  related phase was not found, which implies that Al atoms substitute Zn in the hexagonal lattice and Al ions may occupy the interstitial sites of ZnO or probably Al segregates to the non-crystalline region in grain boundaries and forms Al–O bond [8]. After 100 W i.e. at 150 W in our case we observed that the intensity of (002) peak decreases, may be due to deformation in the grains in the direction of (002) plane.

The transmission spectra of AZO thin film, Fig. 3, shows that at lower power, 80 W, there was a loss of transmission, which can be attributed to the limited solubility of the Al in the film. This is because of the reduction in the deposition rate at lower power. On the increase the RF power, 150 W, the due to the surface scattering of the light, a loss of transmission observed. From the transmission spectra the calculated band gap values of our AZO thin films deposited at different power are higher than the value ( $E_g = 3.25$  eV) of pure ZnO. It is generally believed that the Burstein-Moss effect [9, 10] plays a key role in this phenomenon: ZnO is a natural *n*-type material and the Fermi level would move into the conduction band when it is doped with Al. Since the states below Fermi level in the conduction band are filled, the absorption edge should shift to higher energies. With the sputtering power, increasing from 80 W to 150 W, as Fig. 3 shows, absorption edge shifts negligibly to shorter wavelength observed, which indicates an increase of carrier concentration, known as the Burstein–Moss shift [11]. The variation in the energy band gap and in the absorption coefficient is shown in Fig. 4 (a) and (b) respectively. It was observed from Fig. 4 (b) that, there was a negligible absorption of the photons in the visible region, which could be the important factor for its use as a window layer in solar cell.

The surface morphology of the films i.e. the grain growth, depends upon the deposition flux, which increases, as the RF power increases. Due to that, the surface of the films is becomes denser. The grain growth of the AZO thin films grown at different power clearly observed from in Fig. 5. The surface roughness increases from 17.73 nm to 36.77 nm as the RF power

increases from 80 W to 150 W. The deformation of the grains observed at 150 W RF power is due to the higher deposition rate. The uniformity of the grains of AZO is found at 100 W RF power [11].

Traditionally, in the conduction mechanism of *n*-type ZnO, the intrinsic defects most commonly reported in the literature is the leading background donors in ZnO, namely the oxygen vacancy (Vo) and interstitial Zn (Zn<sub>i</sub>) [12, 13]. For Al-doped ZnO films in our experiments, *n*-type conductivity will be enhanced by Al doping due to the contribution of extra free carriers via Al<sup>3+</sup> ions substituting Zn<sup>2+</sup> ions. The resistivity from four-point probe method was measured to be  $1.5 \times 10^{-3}$ ,  $6.9 \times 10^{-4}$ , and  $4.8 \times 10^{-4}$  Ωcm, when RF power was 50, 100 and 150 W respectively. It indicates that the resistivity decreases with increasing RF power. This, dependence of the resistivity on RF power, leads to an improvement in the nucleation, crystallinity, and the ionized donors, hence a better conductivity, of the films.

#### 4.2 Discussion of working pressure

The XRD spectra of AZO thin films grown at different working pressures, Fig. 6, indicates that on increasing the working pressure from 2 mTorr to 10 mTorr the intensity of the (002) peak increases and by further increment in the working pressure i.e. at 20 mTorr the intensity decrease. In addition, other orientations (101) and (004) are present in the XRD spectra. The improvement in the intensity of (002) peak up to 10 mTorr working pressure shows improvement in the crystallinity of the film, after that the intensity decreases. The crystallite size calculated from the Scherrer formula is 8.16 nm for 20 mTorr working pressure and it is increased as the pressure increases and reaches at the maximum value of 9.66 nm. The variation in the crystallite size, FWHM, d-value and its corresponding 2θ value is tabulated in Table 1. The improvement in the crystalline quality of the films and the crystallite size show the enchantment in the possibility of Al doping in ZnO.

Looking at Fig. 7, the transmission spectra of AZO thin films deposited at different pressure, the drop of the transmittance towards the higher wavelengths indicates that the films were not fully oxidized but it contained metallic (Al) inclusions. It directly impact on the energy band gap of the films. As the pressure increases from 2 mTorr to 20 mTorr the energy band gap decreases from 3.38 eV to 3.31 eV, which is shown in Fig. 8 (a). This behaviour can be explained by examining the dependence of the Al inclusion as a function of working pressure. The variation in the absorption coefficient is shown in Fig. 8 (b).

The AFM images is of the AZO thin films, shown in Fig. 9, the different pressure indicate that the morphology is influence by the working pressure significantly. The grain growth was depending upon deposition flux, which was higher at lower working pressure due to the less scattering probability of the sputtered and gas atoms. Therefore, as the bombardment of energetic particles increases, which leads a non-uniform growth of the grains observed from the AFM images of 2 mTorr pressure. Reduction in the gas pressure results in the decrease of energetic particle bombardment, which was responsible for the uniform grain formation. The increased surface roughness from 19.21 nm to 26.14 nm by increasing the working pressure 2 mTorr to 10 mTorr is likely an indicator of increased grain size, consistent with the X-

ray diffraction data. The variation in surface roughness is tabulated in Table 2.

The variation in the sheet resistance ( $R_{sh}$ ) and the resistivity ( $\rho$ ), from Table 2, suggests that its future use as a front top metallic contact in the CIGS thin film solar cell. As the pressure increases from 2 mTorr to 10 mTorr the  $R_{sh}$  decreases from  $50 \Omega/\square$  to  $23 \Omega/\square$ . At 10 mTorr the resistivity was  $6.9 \times 10^{-4} \Omega\text{cm}$ . The decrease in the sheet resistance can be explained by the increment in the surface roughness of the film. As the roughness increases due to the increment in the average grain size and so, the grain boundary reduces, which decreases the sheet resistance.

## 5. CONCLUSIONS

AZO thin films have been obtained by RF-magnetron sputtering by varying the RF power and the working pressure. Demonstrated structural, optical, electrical, and morphological properties of AZO thin films were analyzed. The obtained films were polycrystalline and had a preferred orientation with the c-axis perpendicular to the substrates. The lowest resistivity of  $6.9 \times 10^{-4} \Omega\text{cm}$  is obtained at 100 W RF power and 10 mTorr working pressure. Transmission measurement shows that all films are highly transparent ( $\sim 85\%$ ) in the visible region. Highly packed uniform grain structure was observed at 100 W at 10 mTorr working pressure. This work demonstrates the future use of Al doped zinc oxide thin films as a window layer as well as a front-contact for the CIGS solar cell.

The authors are thankful to Dr. V. Ganeshan for AFM measurements at the UGC-DAE Consortium for Scientific Research, Indore, and also thankful to UGC-DRS (file No. 530/2/DRS/2007(SAP-1)) for providing a electrical measurement facility.

## REFERENCES

1. T. Nakada, Y. Ohkubo, A. Kunioka, *Jpn. J. Appl. Phys.* **30**, 3344 (1991).
2. O. Kluth, G. Schöpe, B. Rech, R. Menner, M. Oertel, K. Orgassa, H.W. Schock, *Thin Solid Films* **502**, 311 (2006).
3. P. Nunes, D. Costa, E. Fortunato, R. Martins, *Vacuum* **64**, 293 (2002).
4. X.T. Hao, J. Ma, D.H. Zhang, Y.G. Yang, H.L. Ma, C.F. Cheng, X.D. Liu, *Mater. Sci. Eng. B* **90**, 50 (2002).
5. Powder Diffraction File, Joint Committee on Powder Diffraction Standards, ASTM (1998) (Card no. 36-1451).
6. L.V. Azaroff, *Elements of X-ray Crystallography*, (McGraw-Hill, New York, 1968).
7. J.I. Pankove, *Optical Processes in Semiconductors* (Dover, New York, 1971).
8. W. Yang, Z. Liu, D.L. Peng, F. Zhang, H. Huang, Y. Xie, Z. Wu, *Appl. Surf. Sci.* **255**, 5669 (2009).
9. T.S. Moss, *Proc. Phys. Soc. B* **67**, 775 (1954).
10. E. Burstein, *Phys. Rev.* **93**, 632 (1954).
11. D. Song, *Appl. Surf. Sci.* **254**, 4171 (2008).
12. D.C. Look, J.W. Hemsky, J.R. Sizelove, *Phys. Rev. Lett.* **82**, 2552 (1999).
13. D.C. Look, C. Coskun, B. Clafin, G.C. Farlow, *Physica B* **340/342**, 32 (2003).